Composites & nanocomposites

Using particle-loaded inks to selectively change the material properties in binder-jetted WC–Co parts

Maja Lehmann[1,2,*] , Cara G. Kolb[1,2], Josef Gschloessl[1,2], and Michael F. Zaeh[1,2]

[1] *Technical University of Munich, Munich, Germany*

[2] *TUM School of Engineering and Design, Department of Mechanical Engineering,*
Institute for Machine Tools and Industrial Management, Boltzmannstrasse 15, Garching 85748, Bavaria, Germany

ABSTRACT

Functionally graded hardmetals offer a superior combination of fracture toughness and wear resistance and alleviate the compromise that conventional hardmetals must face between these two material properties. In tooling applications, they exhibit superior cutting performance compared to the conventionally employed hardmetals. Traditionally, graded tools are enabled by a surface treatment with nitrogen or carbon. This enables a tungsten carbide–cobalt (WC–Co) tool with a surface layer containing less cobalt (Co) than the core of the part. With this Co gradation, the wear properties can be improved due to the harder surface. If different loads act at different points in a tool and the geometric complexity of a tool increases, the requirements for a targeted positioning of the Co gradients become higher. A simple surface treatment does not allow a flexible distribution of the desired gradients. Binder jetting provides a solution to produce location-independent graded structures. In this work, the process was evaluated for the generation of Co gradients in WC–Co structures. Inks loaded with graphite particle contents of 2.5, 5, 7.5, and 10 m% were used to create differences in the carbon content in the green part. This induced a Co migration during the liquid phase sintering process. The sintering parameters were varied in time and temperature and studied regarding their effect on the microstructure and the porosity, the formation of the Co gradient, and the hardness. At low sintering times and temperatures, all carbon differences led to a Co gradient in the sintering part with a deviation of up to 10 m%. With an increase in sintering time and temperature, the Co distribution began to even out, and a deviation was observed only in the parts created with the inks containing 7.5 and 10 m% of particles. Hardness values of up to 1300 HV10 were obtained, which is comparable to conventionally produced WC–Co parts. The excess of carbon resulted in porosity in the parts leading to a reduced density. However, with inks containing 10 m% particles, densities of 94.26% were achieved at the longest sintering times and the highest temperature.

Springer

Introduction

Tungsten carbide–cobalt (WC–Co) is a widely applied material for the manufacturing of tools for turning, milling, and drilling, for example, in the field of geo-engineering [1]. This is due to its high hardness, the superior wear resistance, and the moderate fracture toughness [2]. However, these properties exhibit an opposing behavior in dependence of the cobalt (Co) content: A higher Co content increases the toughness but reduces the hardness and thus the wear resistance [3, 4]. Functionally graded WC–Co structures offer superior combinations of toughness and hardness, resulting in more durable tools and an improved performance [4]. Accordingly, a Co gradient is targeted in a WC–Co part. The formation of functionally graded WC–Co materials is extensively investigated in previous studies [4–12]. The first to describe the redistribution of the Co in WC–Co was Lisovsky [9]. He introduced the term liquid phase migration. Colin et al. [10] incorporated a graded Co structure in the green part but found out that the Co gradient homogenized after a sintering time of 30 min. Several authors have reported the same observation and stated that having an initial Co difference in a green part leads to a homogeneous cobalt distribution during the liquid phase sintering [2, 6, 11, 13, 14]. However, a pre-designed gradient of the carbon content provides the possibility to create the Co difference during the liquid phase sintering process due to a Co migration [6] and impedes the Co homogenization.

Fang and Eso [2] showed that a carbon gradient in the green part induces a continuous Co gradient during the liquid phase sintering while the carbon content homogenizes. They found that the cobalt migrates from regions with a carbon content above the stoichiometric value toward regions with a carbon content below the stoichiometric value, while the initial Co content was the same throughout the part. The authors explained this effect by a phase reaction, which led to a change in the liquid Co volume fraction. The carbon diffused into a carbon deficient region and the resulting reaction during sintering increased the liquid Co volume fraction and initiated the Co migration. Konyashin et al. [7] also used a spatial carbon difference in the green part to fabricate functionally graded WC–Co. They explained the Co drift by capillary forces resulting from different wettability rates of tungsten carbide (WC) by the liquid Co due to various carbon contents.

Co gradients can also be generated without a carbon difference in the green part. However, this always requires an additional process step, such as a carburizing heat treatment of fully sintered WC–Co parts [4], a denitriding process [4], or the absorption of molten Co into a sintered WC–Co part [9]. Most of the studies on the Co migration focused on the production of surface-to-core gradients, which are generated mainly by surface technologies [4, 7, 15] or in a layer-by-layer mode [8]. This limits the allocation of the gradient to the surface of a part or to complete layers and adds a costly production step to the process chain. An individual local positioning of the gradient and thus an independent adjustment of the mechanical properties in different regions of a part has not been possible so far but can be advantageous for the performance of tools. Considering a milling tool, the cutting surface requires high hardness to increase the wear resistance. Other regions of the tool, such as the shank, are subject to dynamic loads, requiring improved ductility to prevent fracture and to reduce the risk of failure. The binder jetting process provides the possibility to selectively add alloying elements into a green part by using particle-loaded inks. This allows for a locally changed material composition.

Binder jetting is a powder-based additive manufacturing process that uses an ink to selectively solidify the powder particles in one cross-sectional layer of a part. The green part is built layer by layer and the printing process is followed by debinding and sintering to densify the part. This technology enables the production of WC–Co parts with complex geometries, such as internal cooling channels or flow-optimized structures [16]. At the same time, the simultaneous production of several parts is possible [17]. The processing of WC–Co powder during binder jetting was already successfully demonstrated by various authors [18–20]. The addition of particles to the ink during binder jetting allows the voxel-based integration of alloying elements to create tailored material properties [21, 22]. In the case of WC–Co, this means that by using graphite particles in an ink, carbon differences can be introduced into the green part during the manufacturing process. In a previous study, the authors of this work qualified such an ink for the use in the binder jetting process [23].

The aims of this work were to show that the approaches to the Co gradient formation from the literature are transferable to binder jetting and that particle-loaded inks can be used to selectively modify the

material properties in WC–Co structures. These inks were loaded with various amounts of graphite particles to create a carbon difference in the green part. Sintering parameters were varied to investigate the effect of the sintering temperature and time on the carbon diffusion, the microstructure formation, the porosity, the hardness, and the cobalt migration.

Materials and methods

Preparation and characterization of the particle-loaded ink

For the printing of the green parts, the procedure for the preparation of particle-loaded inks, as laid out in Lehmann et al. [23], was used. The inks were specifically designed for the binder jetting process, and the stability and the printability of these aqueous particle-loaded inks have already been demonstrated. The prepared inks were water-based and showed a Newtonian fluid behavior. Particle contents of 1, 2.5, 5, 7.5, and 10 m% were added. Polyvinylpyrrolidone (PVP) (Luvitec 17, BASF, Germany) was added as a dispersant [24] for the nanoparticles in the ink and simultaneously as a binder [25] for the binder jetting process. PVP was dissolved in a water–isopropanol–ethylene glycol mixture for 30 min using a magnetic stirrer to prepare the base ink. For the particle-loaded inks, graphite nanoparticles (Graphite Nanopowder, Nanografi, Turkey) with a mean diameter of less than 50 nm were added, and the water–ethylene glycol ratio was adapted to adjust the viscosity of the inks to meet the requirements of the print head and to ensure a comparability of the behavior of the inks during printing. Sodium hydroxide (NaOH) was used to change the pH value of the inks to maintain a higher dispersion stability [24]. The compositions of the different inks are shown in Table 1. The mixtures were stirred for another 30 min. For the homogenization,

the particle-loaded inks were sonicated for 160 s with a 1-min cooling break after every 20 s. The rheological properties were determined using a rotational rheometer (Kinexus lab +, Netzsch, Germany) with a 40-mm plate–plate geometry and a sample gap of 0.1 mm. The viscosity was measured at a shear rate of $80\,s^{-1}$ for 3 min, capturing 36 single-point measurements. The samples were always kept at a temperature of 25 °C.

The surface tension was studied by the stalagmometric method developed by Traube [26]. Deionized water was used for the calibration. For each of the four performed measurements, 20 drops were weighed. The viscosity and surface tension values are also shown in Table 1. In the further part of the manuscript, the inks are referred to by their carbon content, and the base ink was used as a reference without additional carbon.
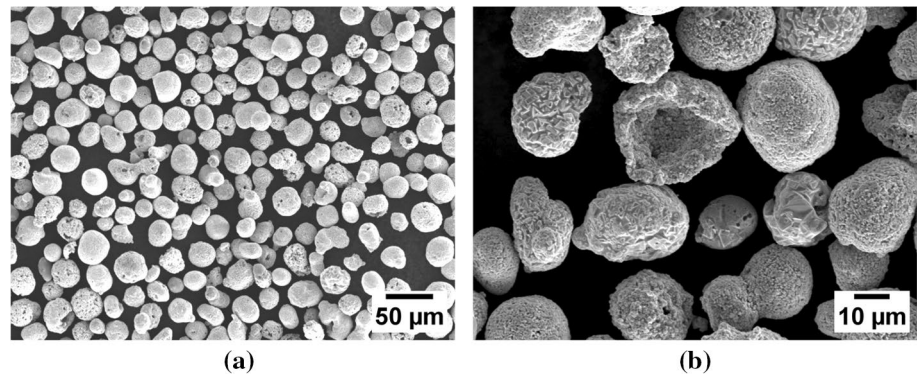
Fabrication of the green parts

For the additive manufacturing of the green parts, spherical WC-12Co powder (AM WC701, Global Tungsten & Powders, USA) with a stoichiometric carbon content of 5.4 m% was chosen. The morphology of the spherical powder is depicted in the scanning electrode microscope (SEM; JSM-IT200 INTouchScope, JEOL, Japan) images in Fig. 1a. The images were taken with a secondary electron detector, a voltage of 20 kV, and a working distance of 11.4 mm. In the close-up (see Fig. 1b), it is noticeable that the sizes of the initial WC grains differ significantly.

The bulk density was determined using a fluorometer (ADP, Karg Industrietechnik, Germany). The particle size distribution was measured with a laser diffraction analyzer (Mastersizer 3000E, Malvern, UK). The flow behavior and the powder layer quality has already been investigated by Schafnitzel et al. [27] and can be found in the assigned publication. The specifications and properties of the powder important for this work are summarized in Table 2.

Table 1 Composition, viscosity η, and surface tension γ of the different inks; EG: ethylene glycol

Ink	Carbon in m%	PVP in m%	Water in m%	EG in m%	Isopropanol in m%	NaOH in m%	η in mPas	γ in mN/m
Base ink	–	13.04	45.87	32.39	8.7	–	7.51	41.11
I2.5	2.5	13.04	45.62	28.34	10.0	0.5	7.05	32.13
I5	5	13.04	48.22	23.29	10.0	0.5	7.13	32.11
I7.5	7.5	13.04	49.75	19.21	10.0	0.5	7.39	32.11
I10	10	13.04	49.75	16.71	10.0	0.5	7.65	32.32

Figure 1 Scanning electron micrographs showing **a** the morphology of the WC–Co powder and **b** the different sizes of the WC grains.

(a)   (b)

Cuboid green parts with a dimension of $15 \times 12.5 \times 10$ mm³ were fabricated with a 3D printer (Voxeljet VTS128, Voxeljet, Germany). A piezoelectric print head (Spectra SL-128 AA, Fujifilm Dimatix, Japan) with 128 individual nozzles, a nozzle diameter of 50 µm, and a nozzle spacing of 508 µm was integrated in the machine. The preparation and the slicing of the digital files were done with the machine software (Rapix3D, Forwiss, Germany). The powder bed was pre-heated to a temperature of 40 °C by an infrared lamp before a new powder layer was deposited. The printing parameters were chosen to achieve geometrical accuracy while still maintaining sufficient strength for handling the green part. The parameters are listed in Table 3. After the printing process, the green parts were dried in a drying furnace (VT 6060 M, Thermo Fisher Scientific, USA) at a temperature of 120 °C for 24 h.

Figure 2 shows the concept that was applied to create a carbon difference in the green parts by binder jetting.

The powder with the constant initial carbon content was solidified by two different inks: the base ink and a particle-loaded ink. The layers of the first half of the part were manufactured with the particle-loaded ink to introduce the excess carbon (referred to as C_+ region), and the subsequent layers were produced with the base ink (referred to as C_0 region). Due to the carbon difference, a Co gradient formation is expected during the sintering process. The Co migrates from the C_+ region to the C_0 region. Depending on the particle

Table 2 Composition and properties of the WC-12Co powder used

Carbon	Co [18]	Bulk density	Theoretical density [19]	D10/D50/D90
in m%	in m%	in g/cm³	in g/cm³	in µm
5.4	12.0	6.25	14.29	7.5/25.4/36.8

Table 3 Parameters used during the binder jetting process

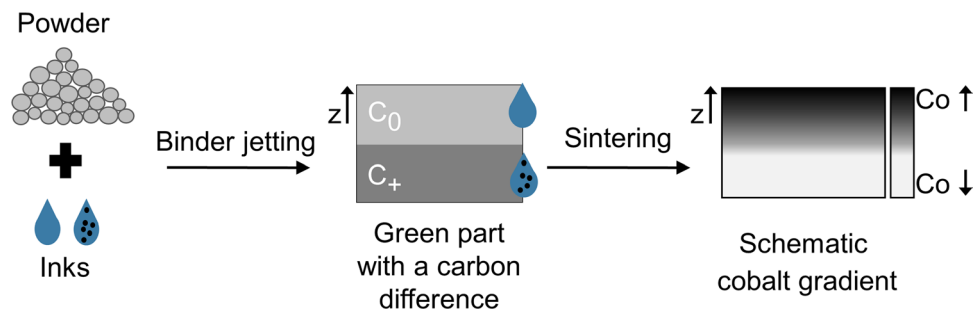| Printing parameter	Value
Printing speed	20 mm/s
Frequency	1000 Hz
Pulse duration	8 µs
Voltage	80 V
Layer thickness	150 µm
Ink saturation	80%

Figure 2 Concept for the creation of a carbon difference in the green part that leads to a cobalt migration during the sintering process; additional carbon was included by fabricating the C_+ region with a particle-loaded ink. The C_0 region was manufactured with the base ink without additional carbon

Table 4 Classification of the different versions of the green and sintered parts according to the inks used in the C_+ region, and the three different sintering conditions applied

Version	Ink	Carbon content in the ink	Sintering condition
–	–	in m%	Temp. in °C / time in min
V0	Base ink	0	1400/25
V2.5	I2.5	2.5	1400/60
V5	I5	5	1450/30
V7.5	I7.5	7.5	
V10	I10	10	

content of the ink, the green parts were divided into different version and 15 parts were printed for each version. The individual terms are listed in Table 4.

Debinding and sintering

The debinding and sintering process was performed in a graphite crucible in a hot-isostatic sinter furnace. The chosen parameters were based on a literature research. For the debinding temperature, the example of Bui et al. [28] was followed. They investigated the burnout time of PVP by a thermogravimetric analysis and observed a complete burnout at 600°C. Therefore, we assumed that no additional carbon is introduced into the green part by the binder. For the debinding, the green parts were heated up to 430°C with a heating rate of 1 K/min. The temperature was held for 1 h and a subsequent heating to 600°C followed with the same heating rate. To prevent the loss of carbon, the samples were exposed to hydrogen gas during debinding. The sintering temperatures were based on Mariani et al. [19]. They sintered at 1400°C and achieved dense WC–Co parts. The sintering times were initially set low to prevent a homogenization of the cobalt and then increased to ensure a higher density. Accordingly, three different conditions were chosen to investigate the effect of the sintering times and the temperature on the carbon diffusion and the Co migration. The sintering temperatures and the holding time at the maximum temperature for each condition are shown in Table 4. Five parts were sintered for each condition. All samples were sintered with a heating rate of 5 K/min in a vacuum atmosphere followed by a hot-isostatic pressure process (100 bar) in an argon atmosphere at the maximum sintering temperature. This was followed by a cooling at a rate of 5 K/min.

Characterization

The images of the WC–Co powder were taken by the SEM. The dimensions of the green parts were measured with a caliper to calculate the geometric density. The Archimedes principle was used to determine the density of the sintered parts for the conditions 1400/60 and 1450/30. For 1400/25, the density was estimated by optical measurements with a threshold analysis (Qness 60 A+ EVO, QATM, Germany), since the Archimedes method was prone to measurement errors at the higher porosity. To further characterize the material properties, the sintered parts were cut along the z-direction, ground, and polished with a 3 µm diamond suspension. The phases and their distribution were analyzed by a light microscope (MM40, Nikon, Japan) and a digital microscope (VHX-7000, Keyence, Japan). The distribution of the Co and the Vickers hardness were measured according to Fig. 3.

The measurements were conducted along the z-direction from the C_+ to the C_0 region and for three rows per part. The measurements at the same height were averaged and the mean values with the standard deviations were determined for all versions. The Co content was determined by energy dispersive X-ray spectroscopy (EDS) analogous to other studies [5, 6]. An acceleration voltage of 20 kV was applied. A magnification of 1200 was used to measure an area of $70 \times 95\,\mu m^2$, and the distance between the areas was 0.35 mm. The hardness of the sintered parts was
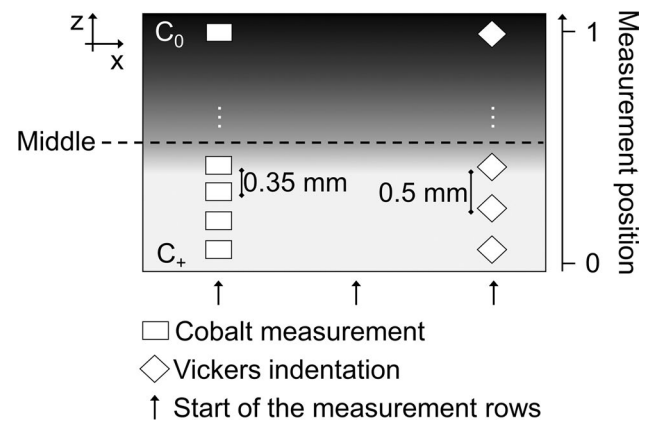

Figure 3 Schematic illustration of the measuring method to determine the average Co content and the Vickers hardness in three rows over the height of the part; the measurement positions were normalized to one to compensate for the shrinkage and to obtain comparable results.

quantified according to the DIN ISO 3878 using the Vickers scale with a load of 1 kg (HV1) and 10 kg (HV10) (Qness 60 A+ EVO, QATM, Germany) with a distance of 0.5 mm between each indentation. Due to the high porosity of some areas of the part, certain measurements points were excluded, since an error-free measurement was not possible for this points.

Results

Density and microstructure

The mean values of the green density (as-built) and the density of all versions before and after the sintering at the three different conditions are depicted in Fig. 4 with the respective standard deviations. In addition, the bulk density of the powder and the theoretical density of WC-12Co are presented as horizontal lines.

The green density lies slightly above the bulk density of the powder for all green parts. After the sintering process, the density for all three conditions increases. For 1400/25, the reference sample V0 shows a density of 12.97 g/cm^3. The addition of carbon reduced the density significantly. V2.5 and V5 exhibit a similar density by about 1 g/cm^3 lower than the reference sample. With a further increase in the carbon content, the density decreases to about 10.70 g/cm^3 for V7.5 and V10. The reference samples for the conditions 1400/60 and 1450/30 are almost fully dense. 1400/60

has a density of 14.16 g/cm^3 and 1450/30 shows a density of 14.25 g/cm^3, respectively, with a standard deviation below 0.06 g/cm^3. For 1400/60, the density decreases for V2.5 to 13.78 g/cm^3, for V5 it increases slightly to 14.03 g/cm^3, and then decreases for V7.5 to 13.60 g/cm^3 and for V10 to 13.25 g/cm^3. The same trend can be observed for 1450/30. The densities of the various versions were marginally higher than for 1400/60. For completeness, the values of the optical density measurements for 1400/60 and 1450/30 are given in Appendix in Table 5.

The occurring porosity that lowers the density is not evenly distributed in the parts, which becomes evident when considering the digital micrographs depicted in Fig. 5.

For the green parts, the gray value difference is clearly visible among the five different versions (see Fig. 5a). The higher the carbon load in the ink was, the stronger the gray value difference between the C_0 and the C_+ region. An increase cannot be observed from V7.5 to V10. This could be due to either a saturation of the gray value or an increased occurrence of clogged nozzles of the print head during the printing process as a consequence of the highly loaded ink. The brighter layers in V5 could also be a result of the clogging of the nozzles.

For the three sintering conditions, the porosity distribution over the parts can be recognized. An accumulation of the pores can be observed along the layer boundaries for 1400/25. For V0, the pores are
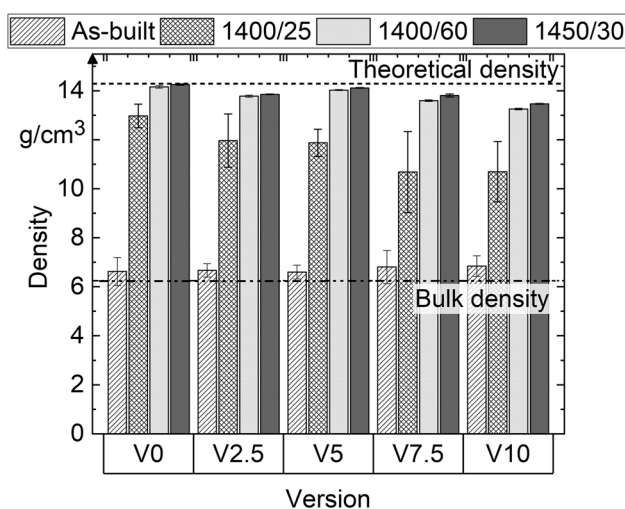

Figure 4 Green density in the as-built state and sinter density for all versions for the three sintering conditions; the bulk density of the powder and the theoretical density of WC–Co are indicated as horizontal lines.

Table 5 Comparison of the density measurements using the optical method and the Archimedes method

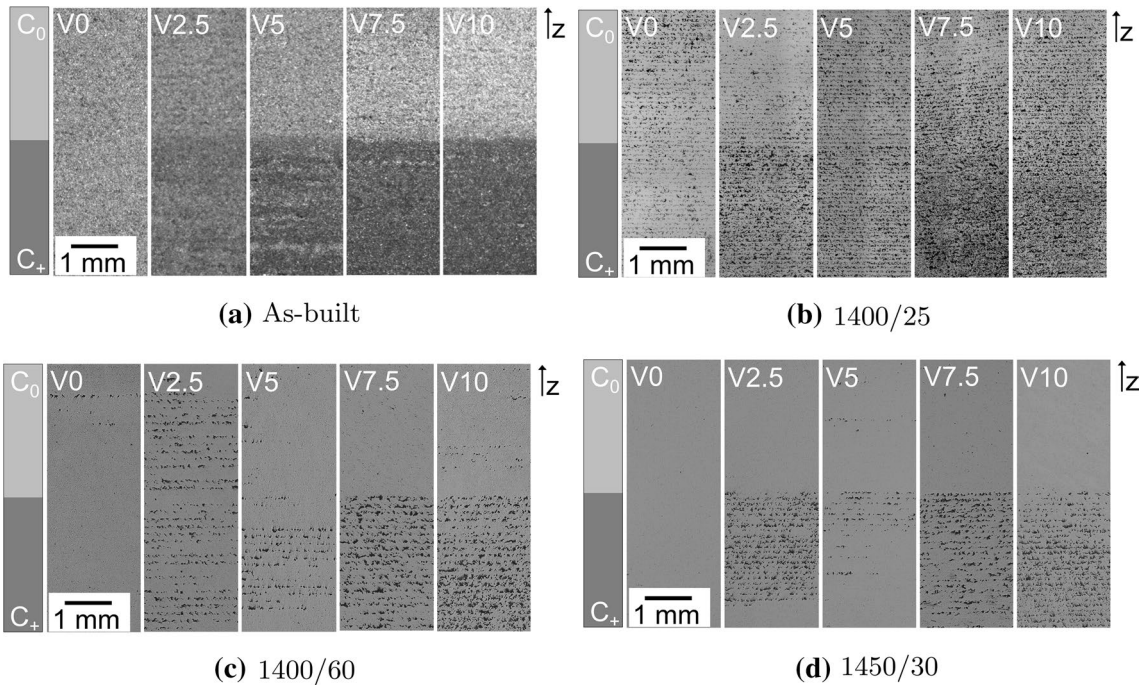| Version	Density in g/cm^3			
	Archimedes		Optical method	
1400/60				
V0	14.16	± 0.05	14.27	–
V2.5	13.78	± 0.05	13.86	± 0.22
V5	14.03	± 0.02	14.26	–
V7.5	13.60	± 0.03	12.55	± 0.91
V10	13.25	± 0.04	13.46	± 0.52
1450/30				
V0	14.25	± 0.03	14.27	–
V2.5	13.85	± 0.01	13.66	± 0.28
V5	14.12	±0.02	14.19	± 0.07
V7.5	13.80	± 0.06	13.76	± 0.23
V10	13.47	± 0.02	13.81	± 0.27

Figure 5 Porosity distribution in the cross section of the **a** green parts and the sintered parts for all versions and for the three different conditions: **b** 1400/25, **c** 1400/60, and **d** 1450/30; the images were taken by digital microscopy.

distributed evenly over the part except for the top of the part. There was no additional carbon in the green part, but a slight carburization may have occurred in the edge area due to the graphite crucible used. The versions with additional carbon exhibit a higher porosity in the C_+ region. The C_0 region of the V2.5 part shows a similar pore distribution as it is the case for the V0 part. For the three other versions, also in the C_0 region, a higher proportion of porosity is present. For V7.5 and V10, a gradation of the pore distribution can be detected, while the pores are distributed homogeneously in the V5 sample.

The reference samples of 1400/60 and 1450/30 show only a little porosity. Some pores are distributed at the edges of the part of the V0 for 1400/60 but the core is fully dense. For the different versions, the pores are particularly present in the C_+ region. The pores in the V2.5 part for 1400/60 appear in both regions but the spacing between the porous lines is increased compared to the V2.5 parts of the other conditions.

Apart from the differences in the porosity, the reference samples of the three sintering conditions show more deviations in their microstructure (see Fig. 6). The WC grains are distributed in the Co matrix. Fine WC grains and coarse WC grain clusters are present under all three sintering conditions. The size of the

fine WC grains differs depending on the sintering conditions. 1400/25 shows the finest WC grains. The size increases for 1400/60 and then grows again for 1450/30. Large pores are visible at 1400/25. At the boundaries of the pores, the cobalt phase accumulates.

Co distribution

Figure 7 shows the distribution of the Co content for all versions and conditions over the height of the parts.

The cobalt content in the reference samples remains constant for all three sintering conditions, but the mean value differs between the three conditions (see Fig. 7a). For 1400/25, the mean cobalt content was 11.04 m% with a standard deviation of 0.28 m%, for 1400/60, the mean cobalt content lies slightly lower at 10.84 m% with a standard deviation of 0.19 m%, and for 1450/30, a mean cobalt content of 11.66 m% with a standard deviation of 0.19 m% was measured. Figure 7b–d displays the cobalt distribution for the parts printed with four versions of the particle-loaded ink at the three different sintering conditions measured in the z-direction. As an orientation, the mean cobalt content of the reference sample is shown as a horizontal line for each sintering
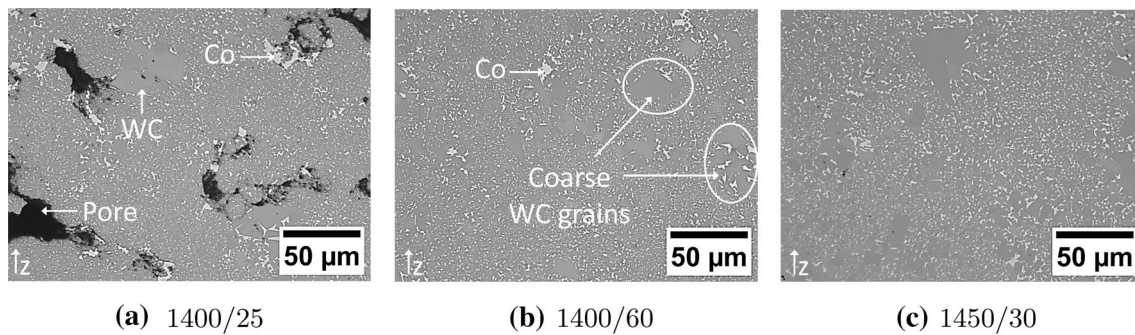
Figure 6 Light optical micrographs of the microstructure of the reference samples for each sintering condition.

condition. At 1400/25, a significant gradation of the cobalt content can be observed for each version.

The Co content in the C_+ region lies under 8 m% for V7.5 and V10. For V5, the minimum Co content is at 8.7 m% and for V2.5 it decreases to 6 m%. Over the height of the part, the Co content increases and lies in the C_0 region above 14 m%, except for V5. The differences in the number of measurement points were due to various heights of the parts. During sintering, the parts shrank at different rates, which is also evident from the variation in porosity.

It is apparent that with increasing sintering time or higher sintering temperature, the gradients are less pronounced or are even homogenized. At 1400/60, no gradient can be observed for V2.5. The measured Co content hardly deviates from the mean value. For V5, the Co content lies slightly below the mean Co content of the reference sample in the C_+ region and marginally above in the C_0 region. The difference in the mean values in both regions is about 1 m%. For V7.5, an increase of around 9.5 m% to around 12.5 m% can be observed and for V10 the Co content rises from slightly below 9 m% in the C_+ region to around 11.5 m% in the C_0 region.

For 1450/30, the Co content is also homogenized for V5 and is also less pronounced for V7.5 compared to 1400/60. The Co content lies constantly below the mean value of the reference sample in the C_+ region and from the middle of the part it approximates the mean value and then slightly rises to values above it. V10 shows a similar behavior. The sudden rise from 9.6 m% to the mean value from measuring position 0.7 to 1.0 in the C_+ region is stronger than for V7.5.

Hardness

Figure 8a shows the Vickers hardness for the reference samples and Fig. 8b and c the hardness distribution for the four versions at 1400/60 and 14,050/30, respectively. Hardness measurements at 1400/25 were not possible, as the porosity was too high and valid indentations could not be obtained. In the regions of high porosity at V7.5 and V10, no valid measurements could be performed according to the standard DIN ISO 3878 due to accumulated porosity. The measured values were excluded because the comparability with the other measured values was not possible and the result would otherwise be falsified.

For the reference samples, the hardness remained constant for all three parameter sets. For 1400/25, the mean hardness was 1255 HV1 with a standard deviation of 100 HV1, for 1400/60 1294 HV10 with a standard deviation of 10 HV10, and for 1450/30 1279 HV10 with a standard deviation of 6 HV10. Due to the porosity of the part, a reduced load of 1 kg (HV1) was chosen for the hardness measurements of the 1400/25 samples. The mean values of the reference samples are also plotted in Fig. 8b and c as a horizontal line. For both sintering conditions, no pronounced hardness gradients can be observed for V2.5. For V5, slight deviations in the hardness can be noted in comparison with the reference measurements. For 1400/60, the hardness is close to the reference value, decreases from the measurement position at 0.4 to 0.53, followed by a light increase at the measurement position at 0.6 and a further decrease at the top of the sample. For 1450/30, the standard deviations of the single measurements

Figure 7 Distribution of the Co content in the reference samples and in the five versions at the three sintering conditions measured in the z-direction; the mean cobalt value of the respective reference sample is displayed as a dash-dotted line.
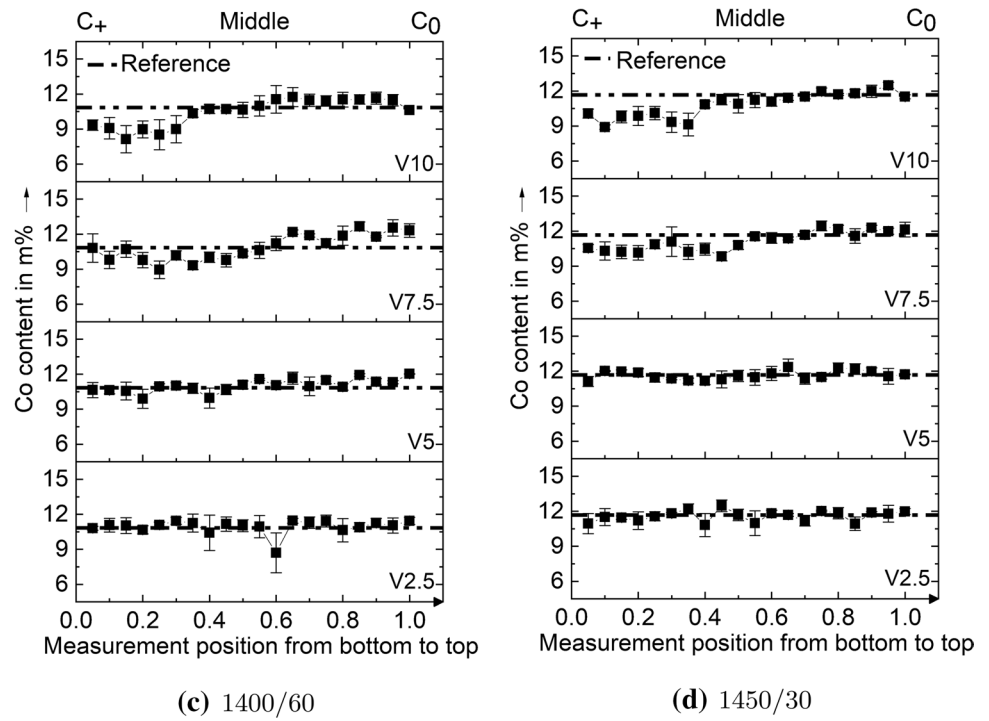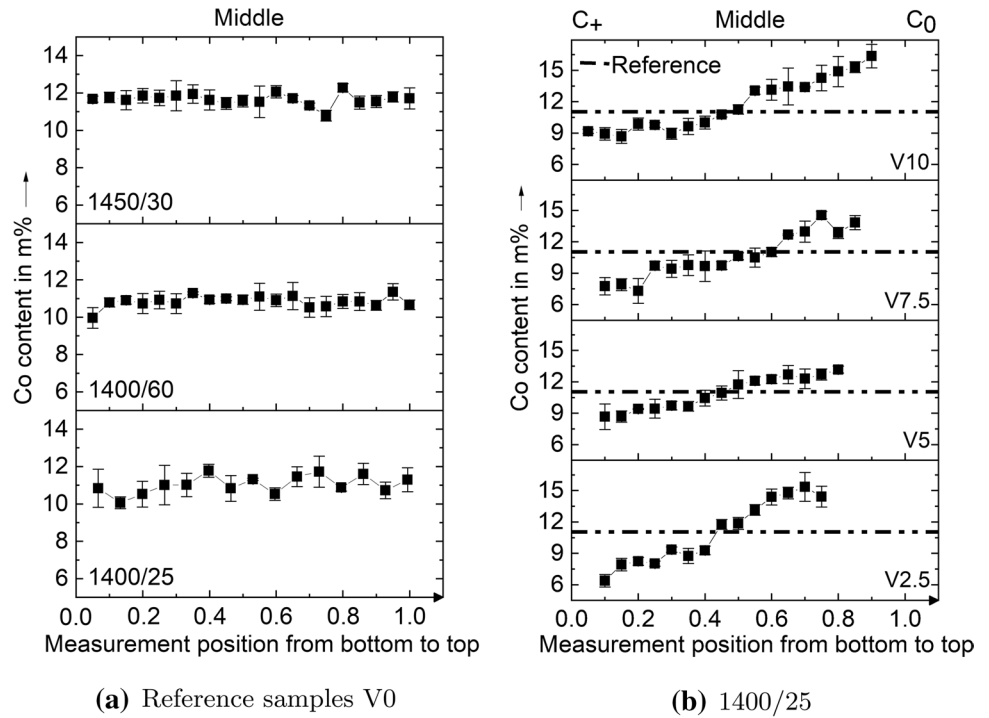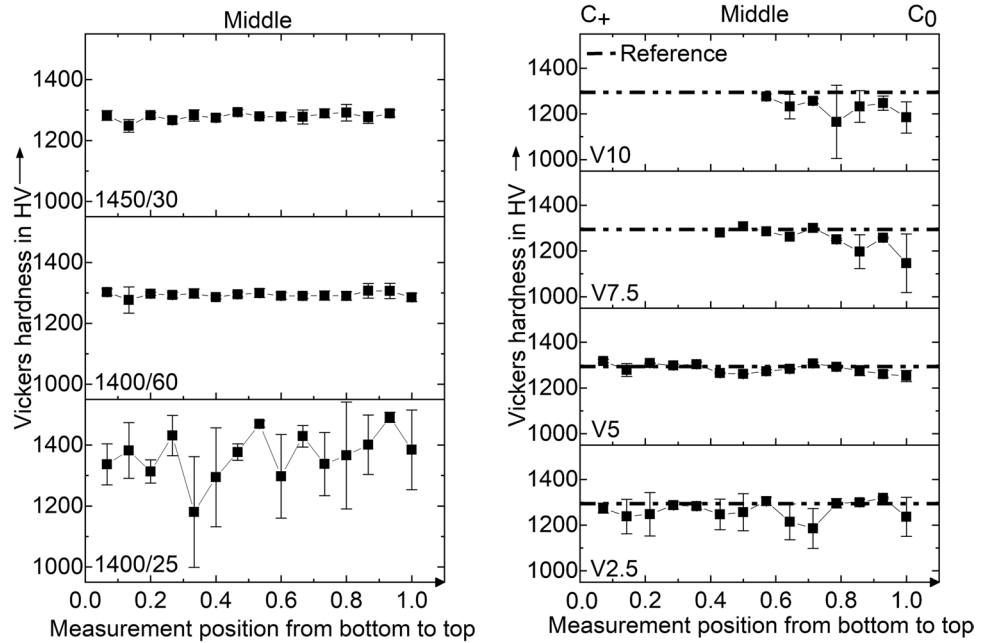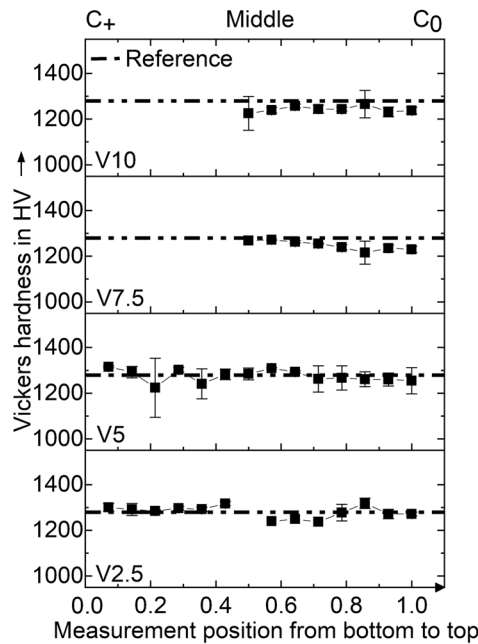

(a) Reference samples V0

(b) 1400/25

(c) 1400/60

(d) 1450/30

Figure 8 Distribution of the hardness in the reference samples and in the five versions at the sintering conditions 1400/60 and 1450/30 measured in the z-direction; the mean value of the respective reference sample is displayed as a dash-dotted line.

(a) Reference samples V0

(b) 1400/60

(c) 1450/30

are higher than for the reference samples, but no gradient can be estimated. For V7.5 and V10 at 1400/60, the measured values from position 0.7 are lower than the reference line at around 1200 HV.

Discussion

The results from the conducted experiments demonstrate that the introduced carbon has an influence on the microstructure, the Co distribution, and the hardness of the sintered WC–Co parts.

Density and microstructure

Porosity

In general, the pore distribution along the layer boundaries described in Sect. 3.1 corresponds to the typical porosity for parts fabricated by binder jetting [19]. The addition of carbon changes the porosity. With an increase in the carbon content in the C_+ region, the porosity of the parts rises. Due to the same green part density for all versions, an influence by the green density on the sinter density can be excluded. Konyashin et al. [7] reported that the carbon content affects the wettability of the WC phase by the liquid Co binder phase. With an increasing carbon content, the wettability by the liquid phase decreases. This leads to a higher capillary force in the C_0 region and the liquid Co is drawn to this region [29]. The reduced wettability impedes the sintering process [30], resulting in a higher porosity. The developed porosity gradient at 1400/25 shows the carbon diffusion. The influence of the carbon content and its diffusion is more pronounced than for the other sintering conditions. At 1400/60 and 1450/30, another effect becomes apparent. The carbon content in the liquid Co phase lowers the solidification temperature [31] and thus changes the progress of liquid phase sintering [32]. This aspect results in an enhanced sintering activity, potentially elucidating the reduced porosity observed at the edges within the C_+ region. However, at the interface where the most pronounced difference of the cobalt content arises, the dominant influence of wettability becomes evident. Therefore, it can be concluded that two effects coincide, which fundamentally influence the porosity. On the basis of the distribution of the pores, it can thus be shown that the difference in the carbon content leads to a diffusion of the carbon from the C_+ region to the C_0 region. The observed differences in the pore distribution throughout the part at the various sintering conditions can be ascribed to the effects described previously. The holistic increased density at 1400/60 and 1450/30 can be attributed to the longer sintering time and the higher sintering temperature, respectively. V5 is an exception at all sintering conditions. The more homogeneous distribution of the pores and the higher density of the parts could be a result of diffusion effects. The diffusion of carbon is influenced by the difference in the concentration. As the carbon affects the proportions
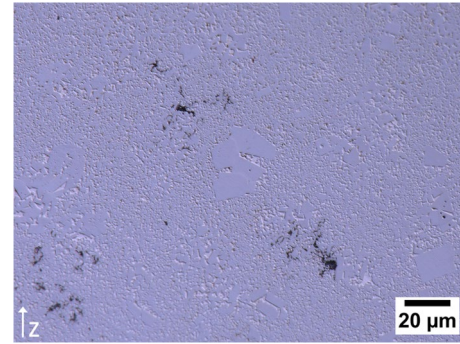

Figure 9 Digital micrograph of the precipitated graphite in the V7.5 part at 1400/60 (black phase).

of the liquid cobalt phase, this in turn influences the carbon distribution, because it diffuses only through the cobalt phase [11]. Thus, the change of the carbon distribution in the various versions could have been a consequence of the interaction of the carbon concentration differences and the amount of the liquid phase formed during the heating process resulting in different driving forces during sintering.

Grain growth

The coarse clusters of the WC grains in the microstructure of all parts have also been observed by other authors [18, 19]. Mariani et al. [19] investigated the powder used and detected coarse-grained particles. They attributed their formation to the overheating of the powder during the spheroidization process, resulting in recrystallization. The use of grain growth inhibitors can help to obtain a homogeneous size distribution [17]. Grain growth effects were observed at a higher sintering temperature and time.

Graphite phase

A carbon content above the stoichiometric value leads to a precipitation of free carbon in the form of graphite in the WC–Co microstructure [32]. This phase reduces the density and the hardness of WC–Co parts [32].

During the phase analysis, the graphite phase was detected in the V7.5 and V10 at 1400/60 and 1450/30. A digital microscopic image showing the graphite phase is depicted in Fig. 9.

V2.5 and V5 did not show any free carbon in their microstructure, leading to the conclusion that the added carbon amount was still below the three-phase equilibrium WC–Co–graphite. In addition, the hardness measurements confirmed the absence of graphite. Since graphite reduces the hardness, it should decrease in the C_+ region in the presence of the graphite phase for V2.5 and V5. However, the hardness was as high or even higher than the reference value.

Co gradient

The results in Sect. 3.2 demonstrated that the introduced carbon differences were able to lead to the formation of a Co gradient in the binder-jetted WC–Co parts. It was shown that the sintering time and the sintering temperature have a great influence on the formation of the Co gradient. They affect the carbon diffusion. The longer the times and the higher the temperatures are, the more carbon must be added to maintain the Co gradient. Fan et al. [6] stated that a holding time of 5 minutes at 1400 °C is sufficient to redistribute and balance out the Co in the part if the carbon difference is no longer present. Konyashin et al. [12] also observed a reduced Co gradient with increasing sintering time. They presumed that, after 60 min of sintering at 1370 °C, the carbon difference between two layers was eliminated.

At 1400/25, the carbon difference was still present in the part. It is assumed that the strength of the porosity gradient can be correlated with the carbon diffusion. Even with a low carbon input, a strong Co gradient of 10 m% was formed. The diffusion of the carbon might also have been hindered by the porosity or the rigid WC skeleton [6] as a consequence of the fewer liquid cobalt phase at the shorter sintering time.

At 1400/60 for V2.5, the Co gradient was already homogenized, for V5 a Co gradient of slightly above 1 m% of Co was generated. At V7.5 and V10, a difference of more than 2 m% was possible. Thus, the carbon difference can be maintained for a longer sintering time at a higher diffusion rate if the initial concentration imbalance is high enough. At 1450/30, the higher sintering temperature resulted in a faster diffusion rate of the carbon and less pronounced gradients were formed.

It appears that a low porosity and a high Co gradient create a conflict of goals. The high porosity that was observed in the binder-jetted parts (see Sect. 3.1) limits the application as a tooling material [33]. The literature has shown that dense functionally graded WC–Co parts are already achievable in conventional processes. Fan et al. [6] attained a minimum porosity in their graded parts after sintering at 1400 °C. Colin et al. [10] reported porosity gradients in solid-state sintered functionally graded WC–Co structures. However, using liquid phase sintering, dense parts were formed. Since an influence of the debinding is unlikely [21], it can therefore be assumed that the high porosity in the binder-jetted parts is attributed to the forming process of the green parts.

Improving the printing process might help to achieve dense parts without reducing the carbon content and thus preserve the Co gradation. A lower layer height and the use of a roller with a larger diameter that spreads the powder during printing can increase the green density and significantly enhance the sinter density [34]. Additionally, the drying time and the binder saturation have a great influence on the green density and a suitable combination can improve the microstructural properties of the sintered parts [20].

Furthermore, the sintering parameter should be chosen in such a way that the time and the temperature are not sufficient to compensate for the carbon difference and are still long enough to achieve dense components with pronounced cobalt gradients.

Hardness

The values of all reference samples follow a constant trend over the height of the part and were comparable with the hardness of conventional WC–Co with medium WC grain size (1.3 – 2.5 µm) [35] and other binder-jetted WC–Co parts from the literature. Enneti et al. [18] obtained a Vickers hardness of 1256 HV30 and Mostafei et al. [20] observed values from 1270 to 1320 HV60 for parts with the same amount of Co. The Vickers hardness 1205 HV10 measured by Mariani et al. [19] was slightly lower than the other values.

Due to the porosity, the load for the hardness measurement for the reference sample at 1400/25 was reduced to 1 kg (HV1). This explains the high standard deviation (see Fig. 8a). The indentations were smaller, and the microstructure differences caused by the coarse clusters of WC grains significantly influenced the hardness measurements.

No strongly pronounced hardness gradients could be detected in the graded versions. There were differences from the mean value of the sintering conditions, but a clear trend was not detectable. However, this
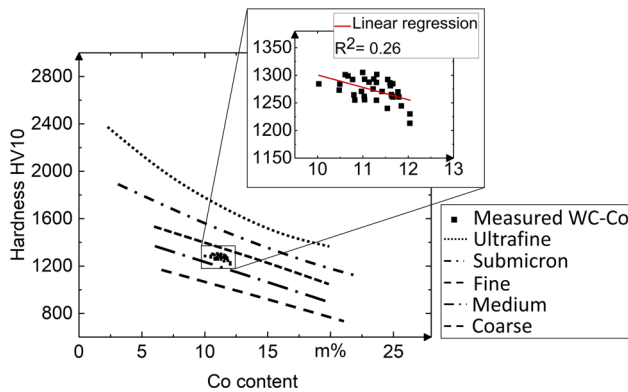
Figure 10 Correlation of the measured hardness and the cobalt content (marked measurements points) in relation to the typical hardness as a function of the Co content for different grain sizes of homogeneous conventional hardmetals; ultrafine: $0.2 – 0.5\,\mu m$, submicron: $0.5 – 0.8\,\mu m$, fine: $0.8 – 1.3\,\mu m$, medium: $1.3 – 2.5\,\mu m$, and coarse: $2.5 – 6.0\,\mu m$ [35]; for the classification of the measured points a linear regression (red line) was used; data for the grain size-dependent hardness for hardmetals adapted from Armstrong [36] and Fraunhofer IKTS [37].

could be caused by the irregularities and limitations in the measurements. The high porosity and the coarse grain growth cause the values to fluctuate strongly, and at higher carbon contents, the porosity was too pronounced to obtain any valid values.

Although the values in the C_+ region for V7.5 and V10 at 1400/60 could not be measured, it can be assumed that the values should be above the reference line, since the additional cobalt, which lowers the hardness in the C_0 region, should result in an increase of the hardness in the C_+ region. The same conclusion can be drawn for the measured values for V7.5 and 10 at 1450/30, but the values in the C_0 region are at 1230 HV to 1260 HV higher than for 1400/60. In order to still be able to evaluate the hardness, corresponding values of all graded structures were correlated with the associated ranges of the individual Co contents (see Fig. 10). The hardness is plotted as a function over the cobalt content for typical WC grain sizes in conventionally produced parts.

The measured hardness values are plotted as measurement points and the resulting linear regression lies between the function for the fine and the medium size WC grains. The high deviation of the results and the low coefficient of determination R^2 can be explained by the coarse WC grain clusters distributed in the microstructure of the binder-jetted parts. However, the correlation between a decreasing hardness with an increasing cobalt content is clearly visible.

Conclusions

This study presents a method to use particle-loaded inks to change the material properties in binder-jetted WC–Co structures. It was shown that inks with various carbon contents can be used to generate a carbon difference in the binder-jetted green parts. Three sintering conditions were tested to evaluate the influence of the sintering time and temperature on the formation of the microstructure as well as the cobalt and hardness distribution in the sintered parts. The findings of this study can be summarized as follows:

- The introduced carbon has an influence on the formation of the microstructure, the Co distribution, and the hardness of sintered WC–Co structures.
- With no carbon addition, a maximal density of $14.25\,g/cm^3$ could be achieved for 1450/30. However, the excess of carbon in the binder-jetted green parts results in porosity in the sintered parts. For higher sintering temperatures and longer sintering times, a density of over 92 % is feasible.
- The carbon diffusion during the sintering process leads to a Co migration. The sintering time and the temperature have a strong effect on the diffusion of carbon and thus on the formation of the Co gradient. At lower sintering times, a Co difference of up to 10 m% can be achieved.
- The carbon content plays an important role in the distribution of the Co. With an addition of 7.5 m% and 10 m% of carbon to the ink, Co gradients can be generated under different sintering conditions. For 1400/60, Co differences of about 3 m% were obtained, and 2 m% were possible for 1450/30. With lower carbon contents, Co starts to homogenize at higher sintering temperatures or longer sintering times.
- The hardness values from 1200 HV1 to over 1300 HV10 are comparable to conventionally produced WC–Co parts with a grain size between fine $(0.8 – 1.3\,\mu m)$ and medium $(1.3 – 2.5\,\mu m)$.

To reduce the porosity to use the additively manufactured parts as tools, the printing and the sintering parameters must be improved. A higher green part density can reduce the sintering time and

temperature, which can counteract the homogenization of the Co gradient and can simultaneously lead to denser sintered parts. Therefore, a variation of the printing parameters or the transfer to a printer with industrial standard could be beneficial. Additionally, the sintering parameters must be adapted to control the carbon diffusion, as this regulates the Co gradient formation. The aim is to sinter under the conditions at which the carbon is balanced, while not homogenizing the cobalt distribution. For this purpose, the exact amount of carbon introduced into the green part, and the distribution of the carbon particles in the powder bed must be known. However, the behavior of particle-loaded inks in the powder bed has not yet been investigated. An a priori determination of the distribution of the carbon particles in the powder bed is needed to support the prediction of the Co gradient formation. This requires an understanding of the powder–binder–particle interactions and will be investigated in further studies by the authors.

With a reduction in the porosity and the maintenance of the cobalt gradient, graded drills can be produced in future to validate the presented concept. An additional integration of complex internal cooling channels could provide information on the potential of the binder jetting technology when compared with a conventionally manufactured drill.

Acknowledgements

Author contributions

ML was involved in conceptualization, methodology, investigation–performing experiments and analyzing data, writing–original draft, writing–review and editing, and visualization. CG was involved in writing–review and editing. JG was involved in investigation–performing experiments. MFZ was involved in resources, writing–review and editing, supervision, project administration, and funding acquisition. All authors have read and agreed to the published version of the manuscript.

Funding

Data and code availability

Not applicable.

Declarations

Conflict of interest The authors declare that they have no known competing financial interests or personal relationships that could have appeared to influence the work reported in this paper.

Ethical approval Not applicable.

Appendix

To ensure comparability, the density for 1400/60 and 1450/30 was also evaluated with the optical measurement method. However, for reasons of effort, for fewer samples than for the Archimedes measurement. It was noticed that the standard deviation in the optical measurement was at least ten times greater than in the Archimedes measurements. The density was underestimated in the optical measurements for the samples with high porosity and underestimated for the samples with lower porosity. However, this was mainly within a range of standard deviation.

References

[1] Ren X, Miao H, Peng Z (2013) A review of cemented carbides for rock drilling: an old but still tough challenge in geo-engineering. Int J Refract Metal Hard Mater 39:61–77. https://doi.org/10.1016/j.ijrmhm.2013.01.003

[2] Fang Z, Eso O (2005) Liquid phase sintering of functionally graded WC-Co composites. Scripta Mater 52:785–791. https://doi.org/10.1016/j.scriptamat.2004.12.008

[3] Upadhyaya GS (2001) Materials science of cemented carbides – an overview. Mater Des. 22:483–489. https://doi.org/10.1016/S0261-3069(01)00007-3

[4] Fan P, Fang ZZ, Guo J (2013) A review of liquid phase migration and methods for fabrication of functionally graded cemented tungsten carbide. Int J Refract Metal Hard Mater 36:2–9. https://doi.org/10.1016/j.ijrmhm.2012.02.006

[5] Emanuelli L, Molinari A, Arrighetti G, Garoli G (2018) Effect of the sintering parameters on the liquid Co migration in WC-Co. Int J Refract Metal Hard Mater 70:202–209. https://doi.org/10.1016/j.ijrmhm.2017.10.014

[6] Fan P, Guo J, Fang ZZ, Prichard P (2009) Design of cobalt gradient via controlling carbon content and WC grain size in liquid-phase-sintered WC-Co composite. Int J Refract Metal Hard Mater 27:256–260. https://doi.org/10.1016/j.ijrmhm.2008.08.002

[7] Konyashin I, Zaitsev AA, Sidorenko D, Levashov EA, Ries B, Konischev SN et al (2017) Wettability of tungsten carbide by liquid binders in WC-Co cemented carbides: Is it complete for all carbon contents? Int J Refract Metal Hard Mater 62:134–148. https://doi.org/10.1016/j.ijrmhm.2016.06.006

[8] Tokita M (2003) Large-Size-WC/Co Functionally Graded Materials Fabricated by Spark Plasma Sintering (SPS) Method. Mater Sci Forum 423:39–44. https://doi.org/10.4028/www.scientific.net/MSF.423-425.39

[9] Lisovsky AF (1990) The migration of metal melts in sintered composite materials. Int J Heat Mass Transf 33:1599–1603. https://doi.org/10.1016/0017-9310(90)90016-N

[10] Colin C, Durant L, Favrot N, Besson J, Barbier G, Delannay F (1993) Processing of functional-gradient WC-Co cermets by powder metallurgy. Int J Refract Metal Hard Mater 12:145–152. https://doi.org/10.1016/0263-4368(93)90064-M

[11] Guo J, Fang ZZ, Fan P, Wang X (2011) Kinetics of the formation of metal binder gradient in WC-Co by carbon diffusion induced liquid migration. Acta Mater 59:4719–4731. https://doi.org/10.1016/j.actamat.2011.04.019

[12] Konyashin I, Ries B, Lachmann F, Fry AT (2013) Gradient WC-Co hardmetals: Theory and practice. Int J Refract Metal Hard Mater 36:10–21. https://doi.org/10.1016/j.ijrmhm.2011.12.010

[13] Eso O, Fang ZZ, Griffo A (2007) Kinetics of cobalt gradient formation during the liquid phase sintering of functionally graded WC-Co. Int J Refract Metal Hard Mater 25(4):286–292. https://doi.org/10.1016/j.ijrmhm.2006.07.002

[14] Fan P, Eso OO, Fang ZZ, Sohn HY (2008) Effect of WC particle size on Co distribution in liquid-phase-sintered functionally graded WC-Co composite. Int J Refract Metal Hard Mater 26(2):98–105. https://doi.org/10.1016/j.ijrmhm.2007.02.003

[15] Fischer U AJ Hartzell E.: Cemented carbide body used preferbaly for rock drilling and mineral cutting. Google Patents. US Patent 4,743,515. Available from: https://patents.google.com/patent/US4743515A/en

[16] Yang Y, Zhang C, Wang D, Nie L, Wellmann D, Tian Y (2020) Additive manufacturing of WC-Co hardmetals: a review. Int J Adv Manuf Technol 108:1653–1673. https://doi.org/10.1007/s00170-020-05389-5

[17] Berger C, Pötschke J, Abel A, Richter HJ, Scheithauer U, Weingarten S (2019) Additive Manufacturing of WC-Co Based Tools. Proceedings of 11th TOOLING 2019 conference, Aachen

[18] Enneti RK, Prough KC, Wolfe TA, Klein A, Studley N, Trasorras JL (2018) Sintering of WC-12%Co processed by binder jet 3D printing (BJ3DP) technology. Int J Refract Metal Hard Mater 71:28–35. https://doi.org/10.1016/j.ijrmhm.2017.10.023

[19] Mariani M, Goncharov I, Mariani D, de Gaudenzi GP, Popovich A, Lecis N et al (2021) Mechanical and microstructural characterization of WC-Co consolidated by binder jetting additive manufacturing. Int J Refract Metal Hard Mater 100:105639. https://doi.org/10.1016/j.ijrmhm.2021.105639

[20] Mostafaei A, Elliott AM, Barnes JE, Li F, Tan W, Cramer CL et al (2021) Binder jet 3D printing–Process parameters, materials, properties, modeling, and challenges. Prog Mater Sci 119:100707. https://doi.org/10.1016/j.pmatsci.2020.100707

[21] Godlinski D, Morvan S (2005) Steel parts with tailored material gradients by 3D-printing using nano-particulate ink. Mater Sci Forum 492:679–684. https://doi.org/10.4028/www.scientific.net/MSF.492-493.679

[22] Persembe E, Parra-Cabrera C, Clasen C, Ameloot R (2021) Binder-jetting 3D printer capable of voxel-based control over deposited ink volume, adaptive layer thickness, and selective multi-pass printing. Rev Sci Instrum 92:125106. https://doi.org/10.1063/5.0072715

[23] Lehmann M, Kolb CG, Klinger F, Zaeh MF (2021) Preparation, characterization, and monitoring of an aqueous graphite ink for use in binder jetting. Materials & Design. 207:109871. https://doi.org/10.1016/j.matdes.2021.109871

[24] Kolb CG, Lehmann M, Lindemann JL, Bachmann A, Zaeh MF (2021) Improving the dispersion behavior of organic components in water-based electrode dispersions for inkjet printing processes. Appl Sci 11:2242. https://doi.org/10.3390/app11052242

[25] Polsakiewicz D (2018) Herstellung keramischer Komposite ueber den pulverbasierten Multi-Material-3D-Druck [Dissertation]. University of the Federal Armed Forces Hamburg

[26] Traube J (1891) Über die Capillaritätsconstanten organischer Stoffe in wässerigen Lösungen. Justus Liebig's Annalen der Chemie. 265:27–55. https://doi.org/10.1002/jlac.18912650103

[27] Schafnitzel M, Lutter-Guenther M, Schlick G (2019) Characterization of Commercially Available WC-Co Powders Used for Laser-based Powder Bed Fusion. Porceedings Euro PM2019 – HM and AM Fusion Processes, Maastricht

[28] Bui HM, Fischer R, Szesni N, Tonigold M, Achterhold K, Pfeiffer F et al (2022) Development of a manufacturing process for Binder Jet 3D printed porous Al2O3 supports used in heterogeneous catalysis. Addit Manuf 50:102498. https://doi.org/10.1016/j.addma.2021.102498

[29] Upadhyaya GS (1998) Cemented tungsten carbides: Production, properties, and testing. Materials science and process technology series. Ceramic and other materials–processing and technology. Noyes Publications

[30] Bhaumik SK, Upadhyaya GS, Vaidya ML (1996) Full density processing of complex WC-based cemented carbides. J Mater Process Technol 58(1):45–52. https://doi.org/10.1016/0924-0136(95)02106-X

[31] Bounhoure V, Lay S, Coindeau S, Norgren S, Pauty E, Missiaen JM (2015) Effect of Cr addition on solid state sintering of WC-Co alloys. Int J Refract Metal Hard Mater 52:21–28. https://doi.org/10.1016/j.ijrmhm.2015.05.002

[32] Nie H, Zhang T (2019) Development of manufacturing technology on WC-Co hardmetals. Tungsten. 1:198–212. https://doi.org/10.1007/s42864-019-00025-6

[33] Enneti RK, Prough KC (2019) Effect of binder saturation and powder layer thickness on the green strength of the binder jet 3D printing (BJ3DP) WC-12%Co powders. Int J Refract Metal Hard Mater 84:104991. https://doi.org/10.1016/j.ijrmhm.2019.104991

[34] Barthel B, Janas F, Wieland S (2021) Powder condition and spreading parameter impact on green and sintered density in metal binder jetting. Powder Metall 64:378–386. https://doi.org/10.1080/00325899.2021.1912923

[35] Prakash L (2014) Fundamentals and General Applications of Hardmetals, Comprehensive Hard Materials. Elsevier, Waltham, p 35

[36] Armstrong RW (2011) The Hardness and Strength Properties of WC-Co Composites. Materials 4:1287–1308. https://doi.org/10.3390/ma4071287

[37] IKTS. Fraunhofer IKTS, editor.: Härte und Bindergehalt von Hartmetallen. Accessed 09 May 2023. https://www.ikts.fraunhofer.de/de/abteilungen/werkstoff_prozesscharakterisierung/sintern_charakterisierung/hartmetalle_cermets/materialentwicklung_hartmetalle_cermets.html